PROCEEDINGS, 47th Workshop on Geothermal Reservoir Engineering
Stanford University, Stanford, California, February 7-9, 2022
SGP-TR-223

Lab-scale structural analysis and poroelastic measurements of rocks from the San Emidio Geothermal Field, Nevada, U.S.

Samantha J. Kleich[1], Matthew Folsom[2], Jesse Hampton[1], Kurt L. Feigl[1], and the WHOLESCALE Team

(1) University of Wisconsin-Madison, 1215 West Dayton Street, Madison, WI, 53706 USA. http://geoscience.wisc.edu;

(2) Ormat Technologies Inc., 6140 Plumas Street, Reno, NV, 89503 USA.

skleich@wisc.edu

Keywords: WHOLESCALE, San Emidio, EGS, poroelasticity, stiffnesses, lab measurements

ABSTRACT

In the WHOLESCALE project we aim to simulate the temporal evolution and spatial distribution of stress in and around the geothermal reservoir at San Emidio, Nevada, United States. To constrain the stress modeling efforts, we perform laboratory measurements of elastic stiffnesses and effective pressure coefficients using oriented rock samples collected from outcrops located near the San Emidio geothermal field.

To help contextualize lab-scale measurements through a field-scale lens, it is important to understand whether lab-scale rock deformation is controlled by structural anisotropy and/or heterogeneity. To that end, we measure ultrasonic velocities, Vp and Vs, at 45-degree increments around the circumference of oriented cylindrical specimens for each rock type. Combining the three-dimensional velocity data with geological and textural descriptions, we address whether the velocity is controlled by heterogeneity and/or anisotropy at the plug scale.

To better model stress in subsurface volumes of a geothermal field, it is also important to obtain accurate estimates of elastic stiffnesses and effective stress coefficients at the laboratory scale; particularly the Biot coefficients which are the effective stress coefficients for volumetric strain in an elastic porous solid. Using the information from the velocity structure and textural descriptions, we physically measure the associated stiffnesses and Biot coefficients to help constrain material behavior predictions within the stress model.

In this paper, we provide a snapshot of the work in progress, including the highlights listed in the Conclusions below. The work presented herein has been funded in part by the Office of Energy Efficiency and Renewable Energy (EERE), U.S. Department of Energy, under Award Numbers DE-EE0007698 and DE-EE0009032.

1. INTRODUCTION

The geothermal field at San Emidio has provided over two decades of data collection, with power first being produced in 1987 (Feigl et al., 2022). Since 1987, three DOE-sponsored projects have been awarded to study the geothermal resource at San Emidio. The first DOE-sponsored project (DOE award DE-EE0002847) conducted exploratory drilling between 2010 and 2014 (Feigl et al., 2020). The second and third DOE-sponsored projects (DOE awards DE-EE0007698 and DE-EE0009032) are currently underway to characterize the geothermal resource at San Emidio and to further investigate stress in the geothermal system. As such, the WHOLESCALE acronym stands for "Water and Hole Observations Leverage Effective Stress Calculations and Lessen Expenses".

The goal of the WHOLESCALE project is to simulate the spatial distribution and temporal evolution of stress in the geothermal system at San Emidio in Nevada, United States. To reach this goal, the WHOLESCALE team proposes to develop a methodology that will incorporate and interpret data from four methods of measurement into a multi-physics model that couples thermal, hydrological, and mechanical (T-H-M) processes over spatial scales ranging from the diameter of a borehole (~0.1 m) to the extent of the entire field (~10 km) and temporal scales ranging from the duration of a micro-seismic event (~1 second) to the typical lifetime of a producing field (3 decades) (Feigl et al., 2022). Four types of observational datasets are proposed to be collected: seismology, borehole image logs, geodesy, and hydrology.

The San Emidio geothermal field is located about 100 km north of Reno, Nevada on the western edge of the Lake Range within the northwestern Basin and Range province. The interaction between the northwestern Basin and Range extensional regime and northern Walker Lane dextral shear is what primarily controls the geologic structure of the Lake Range and San Emidio Desert regions (Faulds et al., 2005; Faulds et al., 2006; Drakos, 2006; Folsom et al., 2020). The San Emidio geothermal system occupies a right step in a North-striking, West-dipping, normal fault zone (Feigl et al., 2022). The San Emidio region is dominated by middle to late Miocene Pyramid sequence volcanic rocks and late Miocene to recent sedimentary rocks, all nonconformably overlying Mesozoic metasedimentary rocks (Figures 1 and 2; Rhodes et al., 2011). The basement Mesozoic metasedimentary rocks of the Triassic-Jurassic Nightingale sequence are mostly phyllite. Nonconformably overlying the metasedimentary basement are two members of the Pyramid sequence; sparsely porphyritic basaltic andesite which overlies tuffaceous and volcaniclastic sedimentary rocks. The basaltic andesites in this region can locally be 500 m or more in thickness (Folsom, 2020). Overlying the Pyramid sequence are younger Quaternary sedimentary rocks consisting of basin fill alluvium, playa deposits, and lacustrine deposits. Younger, Quaternary alteration is present along the San Emidio Fault (Folsom, 2020). Much of the geothermal activity is attributed to fault-hosted permeability associated with dilation along a right step

in normal faulting along the Lake Range that allows for deep circulation of fluids (Rhodes et al., 2010; Rhodes et al., 2011; Teplow and Warren, 2015). In addition, there is a 5 km-long, shallow, range-parallel northward outflow path that lies up-dip of normal faulting in the geothermal field (Matlick, 1995; Rhodes et al., 2011).

To better model the stress in the San Emidio geothermal reservoir, it is important to obtain mechanical and poroelastic rock properties of each lithologic unit (i.e., metasediment, basaltic andesite, etc.). To do this, we use oriented plug specimens from rock samples collected at the San Emidio geothermal site. To limit confusion, the sample scale will refer to the shoebox-sized rock samples collected from surface outcrops in the field and the plug specimen scale will refer to the 1-inch cylindrical specimens cored from these rock samples. We can then measure the elastic stiffnesses and effective stress coefficients at the plug scale on each rock type which can be used to more accurately model stress in the geothermal reservoir. However, to properly determine the correct mechanical and poroelastic rock properties, the plug specimens must be categorized as either isotropic, anisotropic and/or contains heterogeneities. In this paper, our focus is on determining whether plug deformation is controlled by structural/textural anisotropy and/or heterogeneities, which is necessary for properly orienting strain instrumentation and stresses at the laboratory-scale to measure interpretable elastic stiffnesses and Biot coefficients.

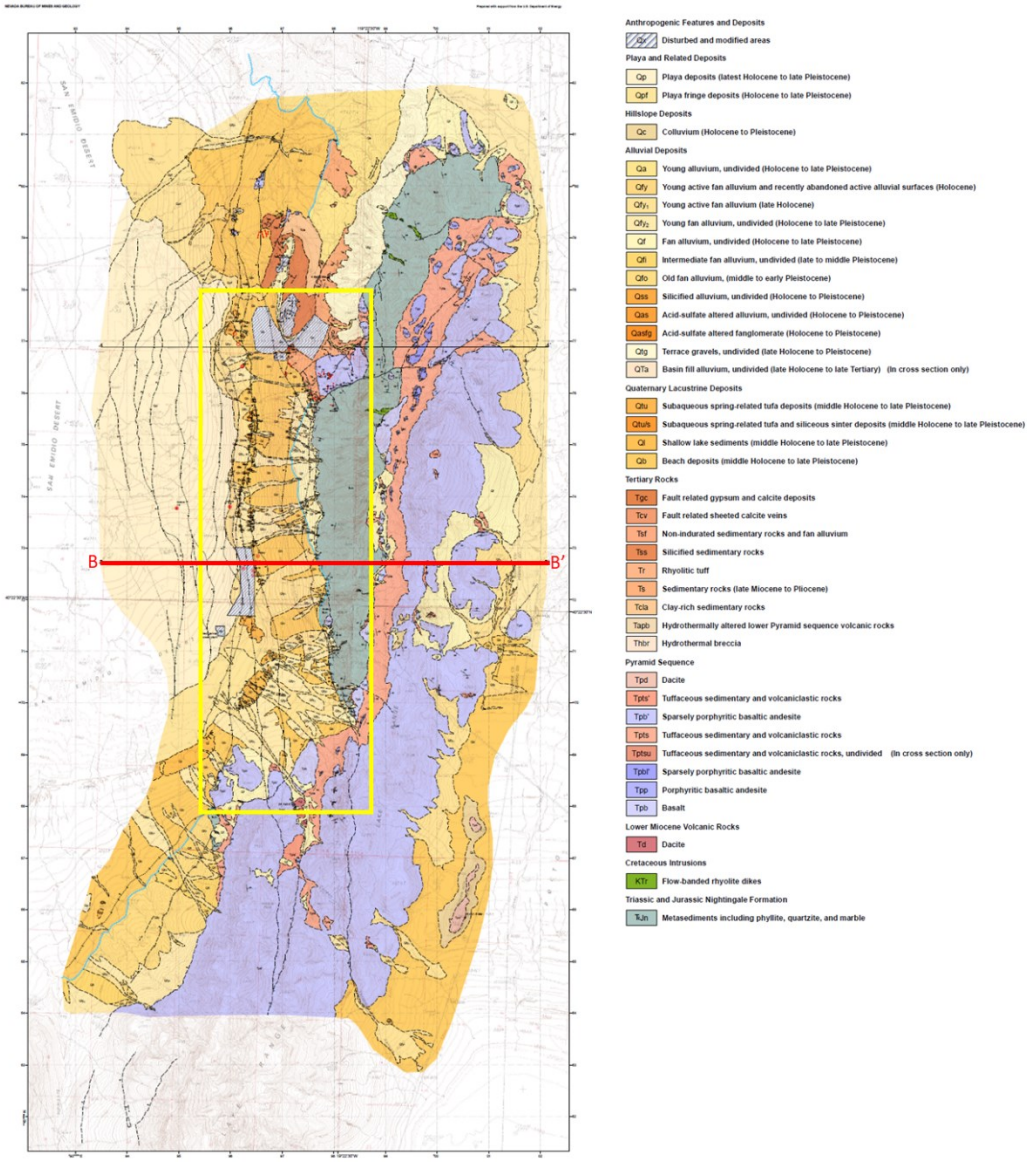

Figure 1. Geologic map of San Emidio (Rhodes, 2011), showing lithology (Rhodes et al., 2011), active geothermal region (yellow), and transect B-B' (red). Coordinates are easting and northing in meters in the Universal Transverse Mercator (UTM), Zone 11, North American Datum 1927 cartographic projection.

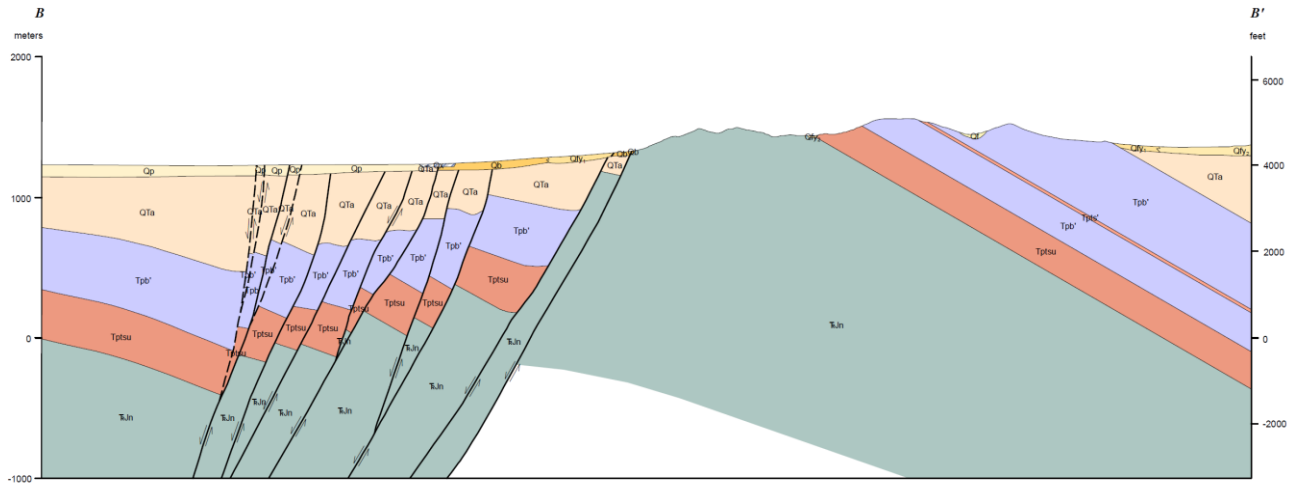

Figure 2. Geologic cross section, showing primary lithologic units and faults. Vertical plane is an E-W transect at Northing coordinate 4472,700 m and Easting coordinates of 293,500 m and 302,200 m (B-B' in Figure 1 shown as a red line). Elevation relative to sea level in meters on left axis and relative to sea level in feet on right axis (Rhodes et al., 2011).

2. METHODOLOGY

2.1 Geological and Textural Descriptions

Materials used in this study were collected from surface outcrops at the San Emidio geothermal site due to the absence of drill core. Therefore, collection of samples from the lithologic units within the area were limited to those that have surface expressions. As a result, these samples are not under the same state of stress as they otherwise would be in subsurface conditions and have been subjected to additional weathering, likely altering the physical properties of the rock materials, including strength and stiffness. Although sample collection and sample condition (i.e., weathering, heavy fracturing) limited the range of samples obtained, a majority of the subsurface lithologic units are represented within this testing suite.

The lithologic units of most concern for this study include QTa (Quaternary basin fill alluvium), Tpb' (Tertiary sparsely porphyritic basaltic andesite), Tpts (Tertiary tuffaceous and volcaniclastic sedimentary rocks), and TrJn (Triassic and Jurassic metasedimentary rocks) due to their location within the geothermal reservoir and their volumetric contribution to the model area (Figure 2). However, because of the lack of surface outcrops and/or integrity of the rock type, QTa and Tpts were not feasible for testing. Therefore, samples of Tpb' and TrJn, as well as Tss (Tertiary silicified sediments) are the primary lithologic units investigated during this study. Estimations of rock properties from wellbore logs, mineralogy, and elemental chemistry will aid in providing constraints for the unmeasured rock types, QTa and Tpts.

Before determining whether a sample was isotropic, anisotropic and/or contained heterogeneities, thin sections were made from numerous rock samples to examine any significant textural or structural features. Three thin sections were made for each rock sample at approximate orthogonal angles to one another (Figure 3). By determining whether one orientation had a more prominent feature than another, we could use this information when coring new samples or infer how this may affect the rock behavior when applying stress. Many of the orientations from each rock sample did not display any noticeable and/or quantifiable fabric (Table 1). Some orientations of TrJn samples contained plagioclase grains that aligned with one another in a linear fashion, whereas other quartz dominated TrJn samples contained a clear gradation from coarse-grained to fine-grained quartz. In addition, few orientations of TrJn contained structural joint patterns. Likewise, a limited number of orientations of Tpb' samples contained a well-defined lineation of plagioclase grains. For the Tss samples, there was a clear interlayering between quartz layers and a fine-grained matrix. However, the fabrics discussed in each of these cases could be dependent on scale and may not be ubiquitous throughout the entire rock sample (i.e., heterogeneity).

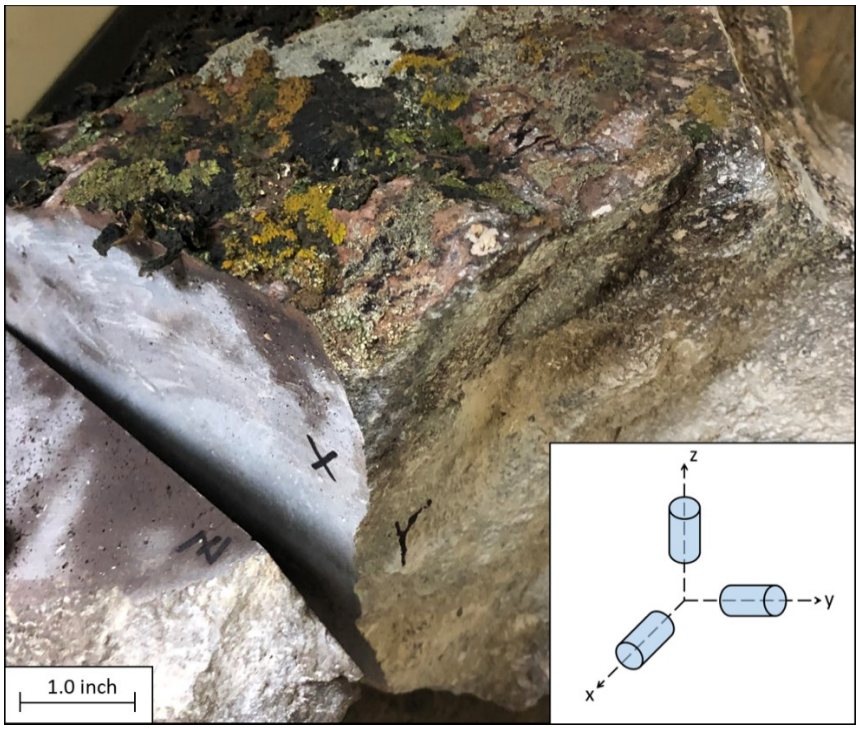

Figure 3. Image of 21KF06 Tpb' sample with markings of X-Y-Z orientations that are approximately orthogonal to one another. Thin sections taken from slabs of each orientation. The inset shows a schematic illustration of plug orientations retrieved from samples. It should be noted that plugs from all three orientations were not taken for every rock sample due to the feasibility of coring and specimen preparation.

Table 1. Three lithologic units of primary interest to this study that were capable of being plugged are shown within the table below. Three thin sections were taken at approximate orthogonal angles for each sample. Orientations (X-Y-Z) of each sample that had quantifiable fabric within thin sections are indicated by a check mark.

Sample ID	Formation (short name)	Formation (long name)	Thin Section Orientation (X/Y/Z)	Quantifiable Fabric from Thin Section
21KF03	TrJn	Triassic and Jurassic Nightingale	X	
			Y	
			Z	
21KF06	Tpb'	Tertiary Porphyritic Basaltic Andesite	X	
			Y	
			Z	
21KF20	Tss	Tertiary Silicified Sediments	X	
			Y	✓
			Z	✓

2.2 Obtaining Plugs for Mechanical and Poroelastic Measurements

To measure mechanical and poroelastic properties of each lithologic unit, we first needed to obtain cylindrical core specimens from the rock samples collected in the field. If possible, three specimens were cored from the same rock sample at approximate orthogonal angles to one another depending on textural/structural information obtained from thin sections (Figure 3). The viability of coring a cylindrical specimen is based on the integrity of the rock samples; for example, degree of weathering, presence of surficial fractures, shape and size of the rock sample (i.e., jagged, small), and rock type. Samples that were heavily weathered, heavily fractured, too small or jagged, or rock types such as tuffaceous and volcaniclastic sedimentary rocks were deemed not feasible to obtain cylindrical specimens, as the preparation process would not result in a testable specimen. Samples considered to be in good condition were used to core cylindrical plug specimens that were 1-inch in diameter and between 1.5 inches to 2 inches in length. The surficial location of these plugs on the sample exterior was free of imperfections and relatively homogeneous. However, in many instances underlying imperfections such as voids and fractures often damaged the plug, rendering it useless, or were visible in the plug specimen. Once the sample is cored and cut to the desired length, each end of the sample is surface ground to achieve parallelism. Parallelism is essential to all types of testing to ensure stress is evenly applied to the sample ends and to inhibit bending of the sample.

Depending on the type of testing being conducted, specimens were jacketed accordingly (Table 2). Two different jacketing methods will be discussed: (1) radial velocity jacketing and (2) copper jacketing. For this study, the radial velocity jacket is used for radial velocity testing and the copper jacketing is used for static stiffness and Biot measurements. A section of viton tubing is used for the radial velocity jacket. This material is a pliable membrane that will contain the sample and prevent leakage of the external fluid used for confining pressure. Two holes are cut 180 degrees from one another in the viton tubing and replaced with radial velocity pucks (Figure 4). It is critical that the pucks sit flush against the specimen surface to properly measure the velocity across the diameter of the plug specimen, therefore curved titanium spacers are used to mate the velocity transducer to the specimens. Epoxy is used to connect the pucks to the viton jacket and fill in any gaps to block leakage. Lastly, each of the jacket ends is secured to the appropriate transducer using annealed steel wire to prohibit leaking. Copper jacketing is used for static stiffness and Biot measurements, as it is a pliable material that conforms to the sample and enables strain gauges to be glued directly to the copper. A piece of 0.13 mm-thick annealed copper sheet is wrapped around the plug specimen and soldered together. After filing down the excess solder, the specimen is placed inside a vessel where the copper is seated to the specimen by applying 13 MPa of hydrostatic confining pressure. Once the strain gauges are applied to the copper surface, the jacketed specimen can be attached to the source transducer and receiver transducer by using viton tubing and steel wire to prevent leaking of the external fluid and internal fluid, like that for the radial velocity jacket (Figure 4).

Table 2. Summary of sample testing. Check marks indicate that a specimen was tested using the method stated in the column heading. Radial velocity testing was conducted on a total of eight specimens discussed during this study. Static mechanical testing and Biot testing was conducted on a total of five specimens for this study.

Sample ID	Formation (short name)	Formation (long name)	Specimen ID	Specimen Orientation (X/Y/Z)	Radial Velocity Testing	Static Mechanical Testing	Biot Testing
21KF03	TrJn	Triassic and Jurassic Nightingale	03-03	X	✓	✓	✓
			03-04	Y	✓	✓	✓
			03-05	Z	✓	✓	✓
21KF06	Tpb'	Tertiary Porphyritic Basaltic Andesite	06-01	Y	✓	✓	✓
			06-02	Z	✓		
21KF20	Tss	Tertiary Silicified Sediments	20-01	X	✓		
			20-02	Y	✓	✓	✓
			20-03	Y	✓		

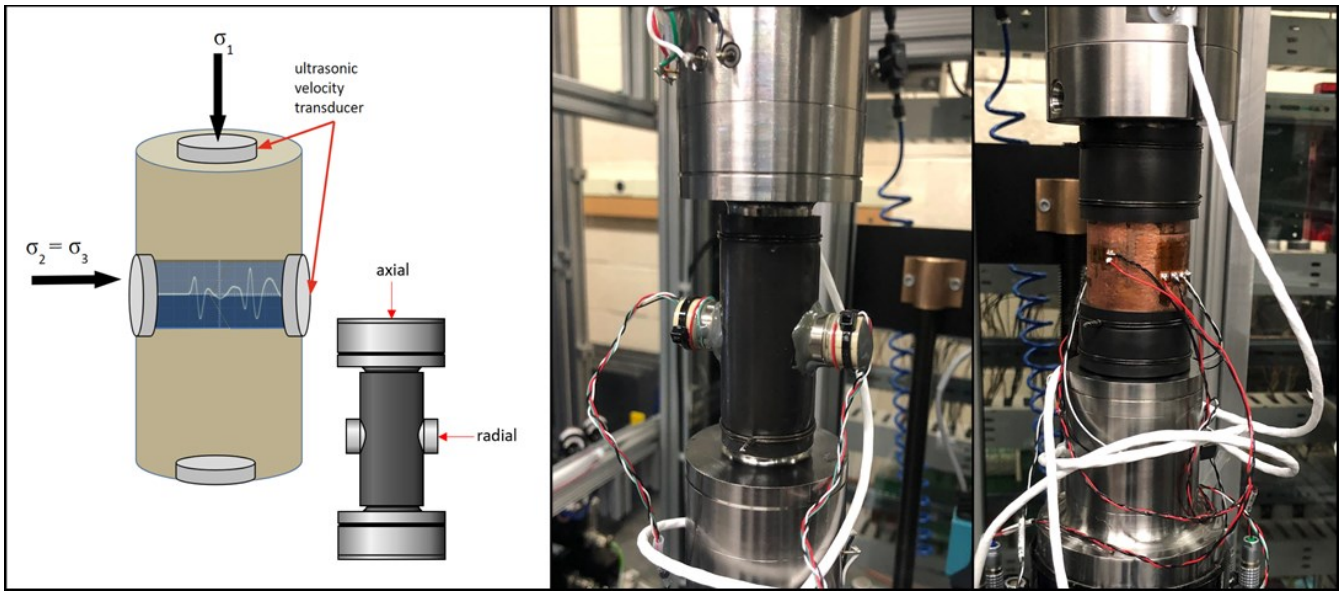

Figure 4. Schematic of radial and axial velocity transducers where $\sigma_1 = \sigma_2 = \sigma_3$ (left). Image of sample stack for conducting radial velocity tests (center). Radial velocity measurements were taken at 10 MPa confining pressure. Image of sample stack for static stiffness and Biot measurements (right).

2.3 Measuring Anisotropy and Heterogeneity at the Plug Scale

Using the viton jacketed sample with the radial velocity transducers, ultrasonic velocities were measured at 45-degree increments around the circumference of the cylindrical plug specimens (Figure 5). The specimens are tested in a high-pressure triaxial testing apparatus with 10 MPa confining pressure applied. A single compressional and two orthogonally polarized shear wave velocities are measured at each orientation to provide valuable information about the lithologic unit, and further compared to axial velocities taken during static mechanical testing. The implications of measuring the velocity at four different orientations pertains to quantifying any anisotropy and/or heterogeneities that may be present within the plug specimen. If the specimen is isotropic (i.e., has a physical property which has the same value when measured in different directions), then the velocity measurements will be approximately the same in all four orientations. If the specimen is anisotropic (i.e., has a physical property which has a different value when measured in different directions), then the velocity measurements would differ between orientations due to interactions with supposed layering, grain texture, fractures, etc.

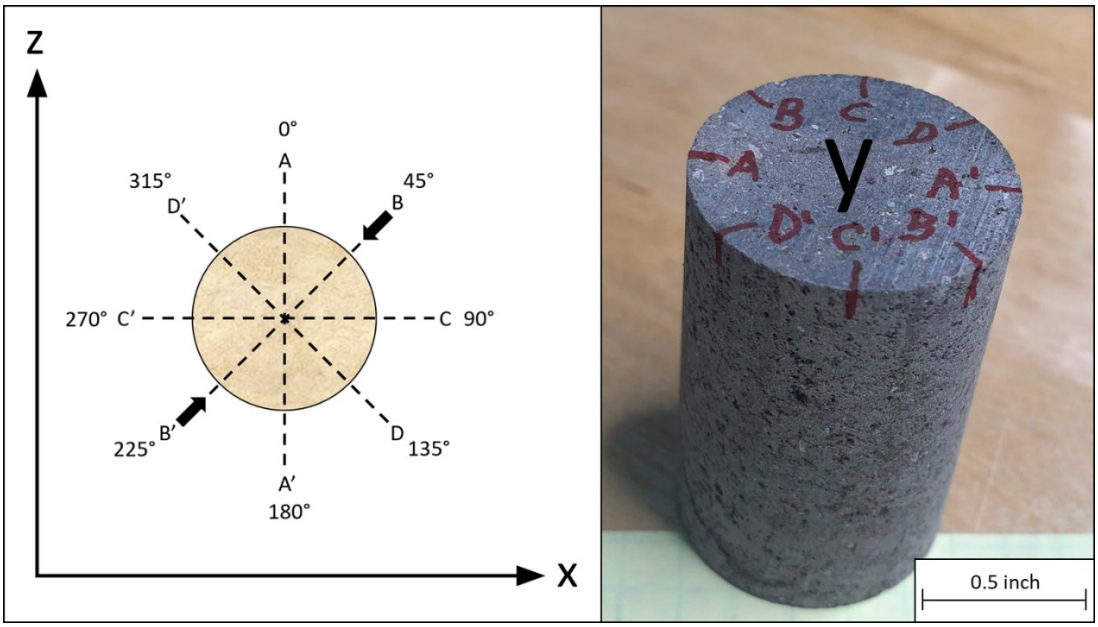

Figure 5. Schematic illustration depicting orientation of radial velocity measurements (left). Image of Tpb' plug sample, 06-01, with markings indicating orientations for velocity measurements (A-A', B-B', C-C', D-D') (right). Plug specimen cored parallel to the y-axis. Four radial velocity measurements were made at 45-degree increments around the circumference of plug specimens.

The combination of qualitatively observing textural and structural anisotropy and/or heterogeneities and quantitatively measuring the radial velocity in four different orientations became useful for a number of reasons. First, geological and textural descriptions from thin sections were used to determine the direction to core the plug specimens. Secondly, by comparing velocity measurements to the thin section descriptions and photographs, we can see if the difference in velocity of a certain orientation is a result of observed fabric. Lastly, if the radial velocity data depicts anisotropy that is not in line with the currently plugged X-Y-Z orientations, we can quantify as necessary and re-core plug specimens in an orientation that would align with the anisotropy.

2.4 Measuring Young's Modulus and Poisson's Ratio

Using the copper jacketing preparation technique, a plug specimen can undergo differential stress, confining pressure, and pore pressure perturbations to measure the associated stiffnesses and Biot coefficients for each specimen. The number of independent elastic constants needed to characterize each rock type is dependent on the categorization made by the radial velocity data and geological/textural descriptions. If a sample is isotropic, only two independent elastic constants are needed to characterize that material (i.e., one Young's modulus and one Poisson's ratio). In contrast, if a sample is characterized as transversely isotropic (i.e., a material with physical properties that are symmetric about an axis that is normal to a plane of isotropy), five independent elastic constants are needed to characterize the material (i.e., two Young's moduli and three Poisson's ratios).

To conduct static mechanical testing, a sample is placed into the triaxial testing apparatus. A confining pressure of 20 MPa and a differential stress of 5 MPa is applied. The sample is then subjected to four different cycles to measure different moduli: (1) Bulk cycle to obtain Bulk Modulus, K; (2) Unistress cycle to obtain Young's Modulus (E) and Poisson's ratio (n); (3) Shear cycle to obtain Shear Modulus, G; and (4) Hydrostatic cycle. The Bulk cycle modulates confining pressure only, the Unistress cycle will ramp differential stress only, and the Shear cycle and Hydrostatic cycle modulate both confining pressure and differential stress (Figure 6). In this paper, our focus will be on measurements of Young's Modulus and Poisson's ratio. Using radial velocity data and the Unistress cycle data, we can respectively obtain dynamic and static E and n for isotropic specimens.

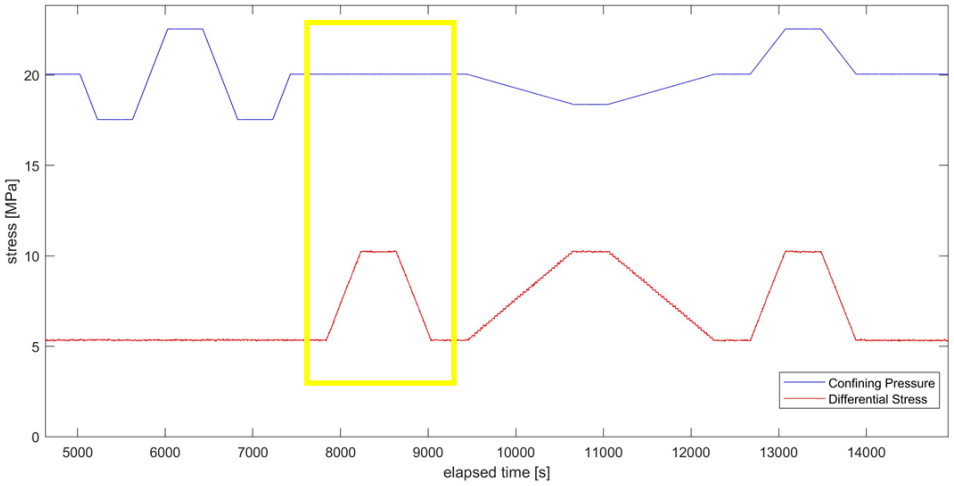

Figure 6. Protocol for static stiffness measurements. Unistress cycle used to obtain static E and n for isotropic specimens is highlighted in yellow. A ramp of 5 MPa differential stress is applied in this case.

3. RADIAL VELOCITY MEASUREMENTS

Here we present evidence from laboratory experiments characterizing each cylindrical specimen and overall lithologic unit as either isotropic or anisotropic. In addition, we will denote if specimens display evidence of heterogeneities that would affect testing results. This will be done using radial velocity measurements, as well as geological and textural descriptions from thin sections. From this analysis, we will show that ultrasonic radial velocity testing is a valuable tool for detecting mechanical anisotropy. The characterizations made within this study will be used when analyzing data from further rock mechanics testing.

Four radial velocity measurements were made on each cylindrical specimen at 45-degree increments around its circumference. Therefore, measurements were made at 0, 45, 90, and 135 degrees (Figure 5). An increment of 45 degrees was chosen as it provided an accurate representation of the possible velocity variations while maintaining a practical testing schedule. Picks of P-wave velocity, S1-wave velocity, and S2-wave velocity were chosen based on the head-to-head picks from a standard 1-inch aluminum sample, to accurately remove transit times within the titanium pucks when rock materials are tested. An example of ultrasonic waveforms with their corresponding velocity picks are displayed in Figure 7. Waveforms did not always result in a well-defined picking location, which can be attributed to the complexities and variations that come from using imperfect rock samples collected in the field. The ramifications and solutions for overcoming complications in velocity picking will be discussed in a later section.

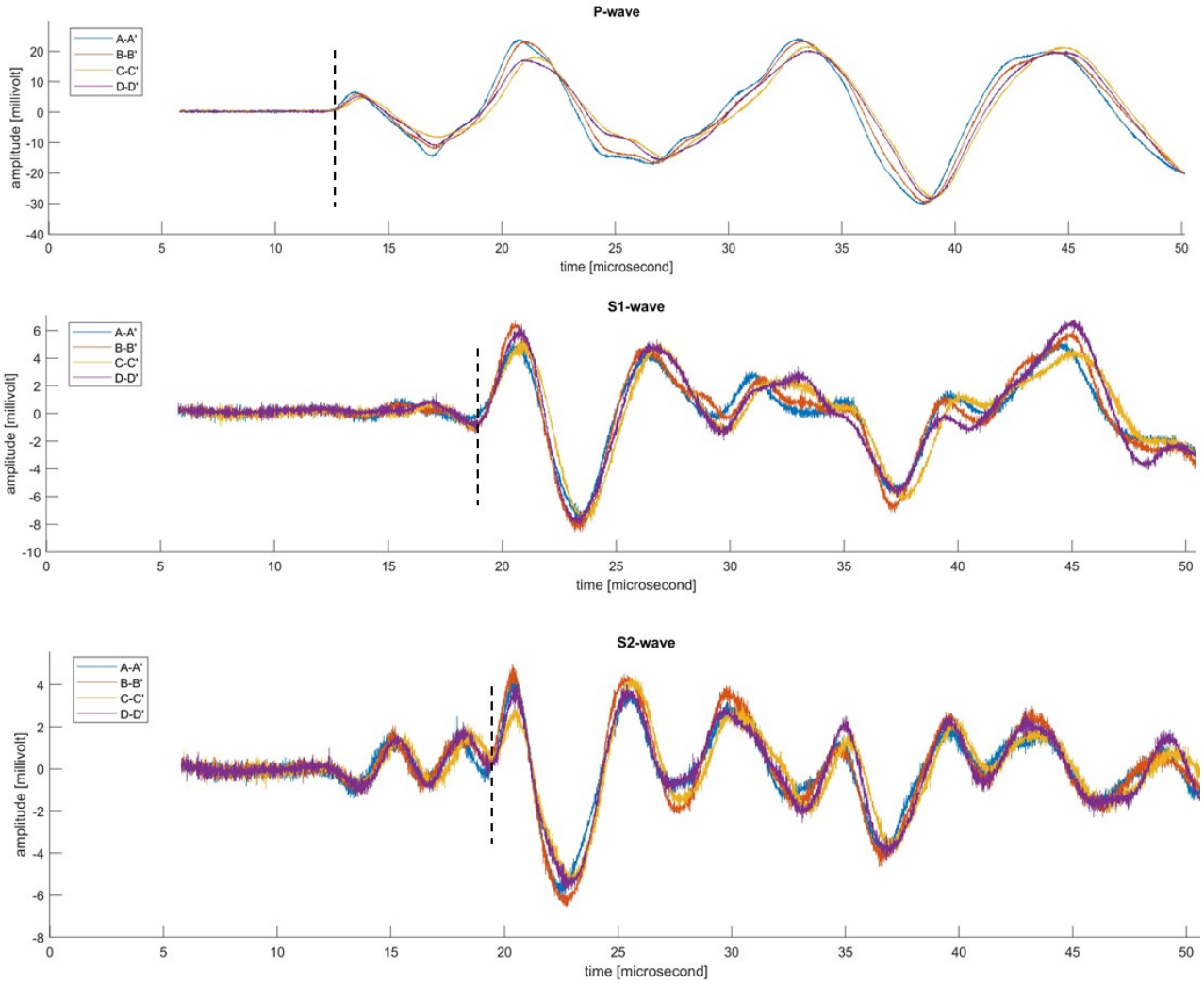

Figure 7. Example ultrasonic radial velocity waveforms of Tpb' specimen, 06-02. P-wave seismogram (top), S1-wave seismogram (middle), and S2-wave seismogram (bottom). Velocities taken at 45-degree increments around circumference of specimen in orientations A-A' (blue), B-B' (orange), C-C' (yellow), and D-D' (purple). Dotted black line indicates position of picked velocity. This test was conducted under a confining pressure of 10 MPa.

Table 3 provides a summary of radial velocity testing for specimens from lithologic units that were of prime interest to the San Emidio geothermal reservoir (i.e., Tpb', TrJn, and Tss) due to their volumetric component. Overall, most samples appear to be isotropic and display very few signs of anisotropy. This is quantified by the differences in velocity measurements between the four orientations tested. Samples that had velocity differences of 250 m/s or less between orientations were classified as isotropic. Samples that had velocity differences of greater than 250 m/s were flagged as potentially being anisotropic and/or containing heterogeneities. Using 250 m/s is a judgment call as it is approximately 6% of the observed velocity values, considering the overall average velocity value measured from all specimens was about 4,000 m/s. For example, if a P-wave velocity pick at the 0-degree orientation was 3,900 m/s and at the 45-degree orientation was 3,830 m/s, then this would be a difference of 70 m/s and classified as isotropic. If this difference was more than 250 m/s, say between velocities of 3,900 m/s and 4,300 m/s, then the sample would be further investigated for anisotropy and/or heterogeneities. One way of visualizing this is by plotting data on a polar diagram which will be discussed in more detail later in the paper. Samples that are isotropic will have similar velocity values and thus, the shape of the radar chart will be more uniform and circular in shape. Samples that are anisotropic will have velocity values that significantly differ from one another and thus, the radar chart may be more irregular or oblong in shape. However, this is dependent on the scale being used to compare velocity measurements. In addition to comparing orientations from the same cylindrical specimen, a comparison of velocities can be made between different plug orientations from the same rock sample (i.e., X, Y, Z). The same criteria of a difference of 250 m/s in velocity is used for comparing velocities across plug specimens.

Table 3. Summary table of radial velocity testing of plug specimens. Table includes designation of specimen orientation, the ultrasonic velocity measurements at each direction (i.e., 0, 45, 90, 135), average radial velocities and standard deviations for each specimen, and the classification assigned on a plug-scale based on radial velocity measurements along with geological/textural descriptions. Averages and standard deviations are obtained from four ultrasonic velocity measurements made at each direction around the circumference of the specimen at one picking location on the seismogram.

Sample ID	Specimen ID	Specimen Orientation (X/Y/Z)	Angle [degrees]	P-wave [m/s]	S1-wave [m/s]	S2-wave [m/s]	P-wave		S1-wave		S2-wave		Specimen Classification (Isotropic/Anisotropic)
							Average [m/s]	Standard Deviation [m/s]	Average [m/s]	Standard Deviation [m/s]	Average [m/s]	Standard Deviation [m/s]	
21KF03	03-03	X	0	6013	3538	3671	5971	45	3508	30	3646	15	Isotropic
			45	6011	3538	3644							
			90	5959	3474	3633							
			135	5902	3482	3636							
	03-04	Y	0	5788	3582	3338	5797	58	3534	50	3333	21	Isotropic
			45	5893	3585	3334							
			90	5739	3501	3359							
			135	5766	3469	3302							
	03-05	Z	0	6102	3684	3812	5945	95	3601	69	3768	54	Isotropic
			45	5905	3542	3814							
			90	5846	3524	3767							
			135	5926	3653	3680							
21KF06	06-01	Y	0	4821	2535	2647	4701	73	2518	27	2643	19	Isotropic
			45	4668	2495	2643							
			90	4624	2488	2613							
			135	4690	2553	2667							
	06-02	Z	0	3912	2246	2197	3884	33	2247	12	2182	15	Isotropic
			45	3872	2263	2196							
			90	3835	2249	2160							
			135	3915	2229	2176							
21KF20	20-01	X	0	5238	2965	3106	5205	28	2981	12	3089	14	Isotropic
			45	5225	2977	3073							
			90	5190	2986	3078							
			135	5168	2996	3100							
	20-02	Y	0	5158	2938	3074	5213	51	2965	18	3116	42	Isotropic
			45	5292	2969	3183							
			90	5222	2988	3116							
			135	5182	2966	3089							
	20-03	Y	0	5193	2965	3057	5194	13	2969	7	3050	6	Isotropic
			45	5212	2968	3046							
			90	5194	2962	3055							
			135	5176	2981	3044							

One specimen was classified as having a velocity difference of greater than 250 m/s. Specimen 03-05, was slightly over a difference of 250 m/s with a P-wave velocity difference of about 256 m/s between the 0-degree orientation and the 90-degree orientation. However, the percent difference between the fastest and slowest velocity orientations was still very small. The percent difference between the fastest P-wave velocity and the slowest P-wave velocity was about 1.04% and therefore, the sample is still considered isotropic.

Between plug specimens from the same rock sample (i.e., specimens 03-03, 03-04, and 03-05 from sample 21KF03), a larger variation in velocities was found. Therefore, this may indicate anisotropy at the sample scale that is not apparent at the plug scale. Using velocity measurements displayed in Table 3, the largest differences between P-wave and S-wave velocities amongst all specimens from a rock sample (i.e., 21KF03) were considered. For sample 21KF03, a TrJn sample, the largest P-wave velocity difference was 363 m/s and the largest S-wave velocity difference was 512 m/s between three plugs in three different orientations: X, Y, and Z. For sample 21KF06, a Tpb' sample, the largest P-wave velocity difference was 986 m/s and the largest S-wave velocity difference was 507 m/s between two plugs in two different orientations: Y and Z. The large velocity differences between plug samples of the same rock type could indicate either anisotropy or heterogeneity at the rock sample scale. For sample 21KF20, a Tss sample, there was not a significant velocity difference between plugs from the same rock, thus indicating isotropy throughout the rock sample. The largest P-wave velocity difference was 134 m/s and the largest S-wave velocity difference was 246 m/s for three plugs in two different orientations: one in the X-orientation and two in the Y-orientation.

To confirm the presence of anisotropy within a sample with significant velocity differences, fabrics were analyzed within thin sections to compare to the measured velocity values. In rock samples 21KF03, 21KF06, and 21KF20 the results are quite interesting. Although the velocity differences are significant between plug orientations for samples 21KF03 and 21KF06, the thin sections do not display any quantifiable or noticeable fabric that can explain the apparent mechanical anisotropy. For sample 21KF03, the thin section is described as having equigranular quartz grains that are not elongated in any preferential direction and no layering is visible (Figure 8). For sample 21KF06, the thin section is described as having plagioclase grains that are rarely aligned with one another and many void spaces that are not elongated in any preferential direction (Figure 9). If plagioclase grains were lineated or quartz grains were elongated, this could explain the velocity differences. In contrast sample 21KF20, which had relatively consistent velocity measurements between plug orientations, does display evidence of a quantifiable fabric in thin sections. Although dependent on scale, the interlayering between quartz-grain layers and a finer-grained matrix could result in sample anisotropy for sample 21KF20, yet this is not indicated through velocity measurements (Figure 10).

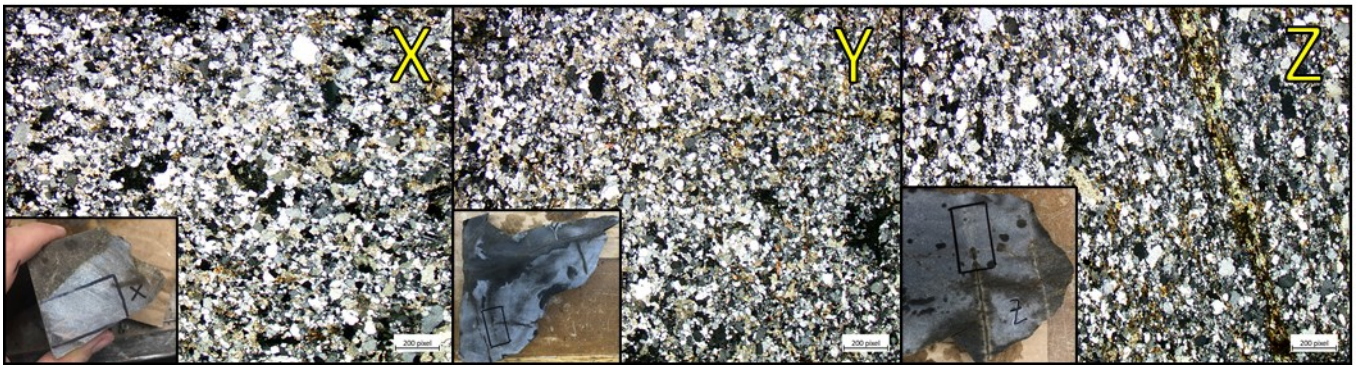

Figure 8. Thin section images from TrJn sample, 21KF03, at three approximate orthogonal orientations. X-orientation (left), Y-orientation (center), and Z-orientation (right). All orientations display fairly equigranular quartz grains with small masses of fine-grained biotite and muscovite throughout. Few cross-cutting fractures throughout thin sections.

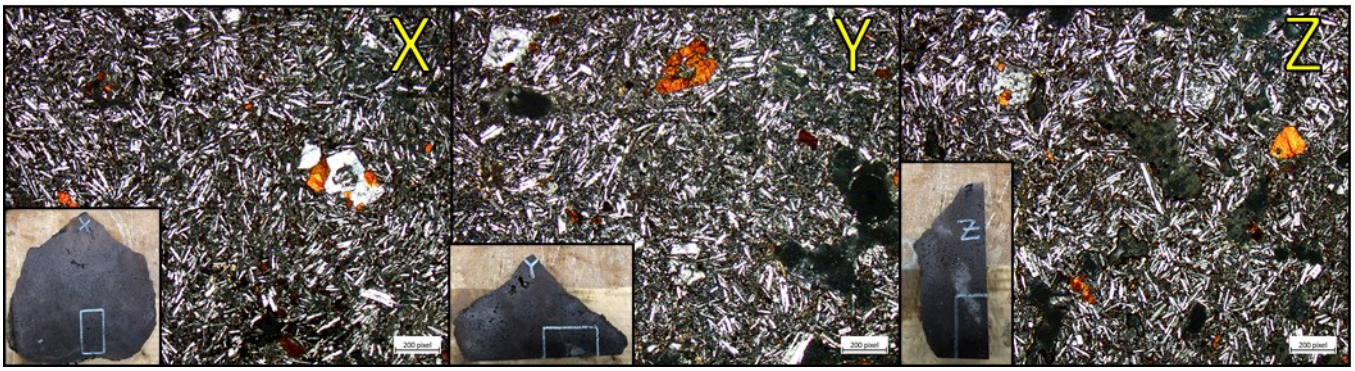

Figure 9. Thin section images from Tpb' sample, 21KF06, at three approximate orthogonal orientations. X-orientation (left), Y-orientation (center), and Z-orientation (right). All orientations display chaotic orientation of plagioclase grains with no clear lineated pattern. Many void spaces within thin section on account of being a vesicular basalt, but no preferential direction of elongation. Some larger plagioclase and clinopyroxene phenocrysts throughout thin section.

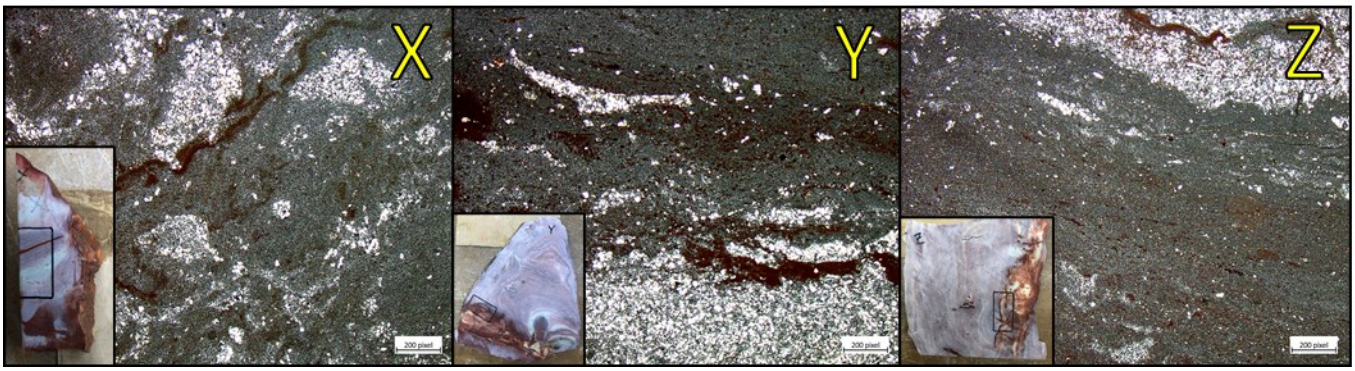

Figure 10. Thin section images from Tss sample, 21KF20, at three approximate orthogonal orientations. X-orientation (left), Y-orientation (center), Z-orientation (right). X-orientation displays clasts of fine-grained quartz within grey fine-grained matrix and some linear red iron-stained features. No clear elongation of grains or layering. Y- and Z- orientations both display interlayering between fine-grained quartz and grey/dark red iron-stained matrix. Although these linear features are present on the thin-section scale, they may not be representative or ubiquitous throughout the sample scale.

However, as mentioned previously, there were oftentimes complications when picking velocities. Frequently, a waveform did not have a well-defined pattern or arrival pick location that resembled that of the head-to-head waveform. This could lead to errors in the velocity differences mentioned above and may over- or under-predict the velocity differences, thus altering the classification of isotropic or anisotropic. To quantify the error brought about by picking, velocities were picked at multiple locations representing possible arrival energy. This allowed us to give a range of possible velocities for each specimen rather than assigning it a single velocity value (Figure 11).

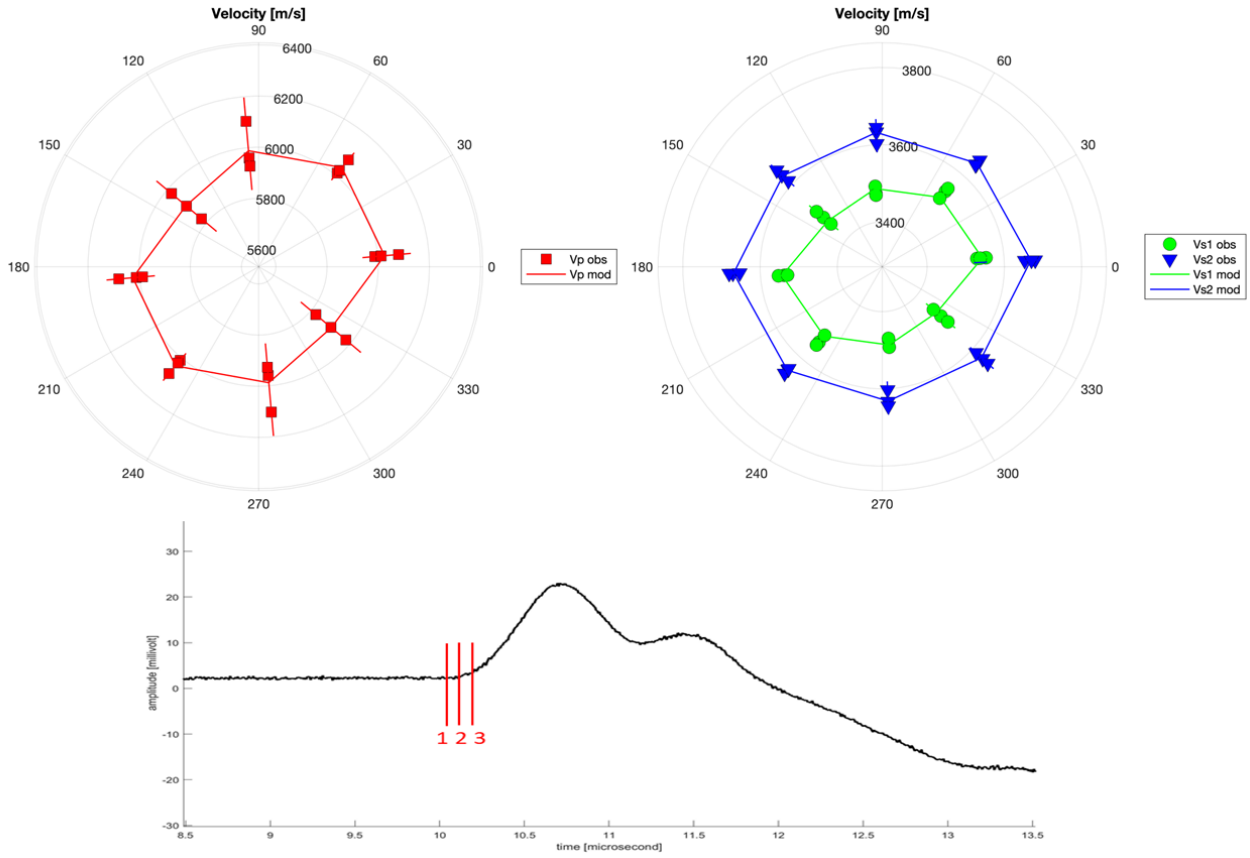

Figure 11. Polar plots of velocity picks from TrJn sample, 03-03. Observed P-wave velocity picks indicated by red squares (top left). Observed S1-wave velocity picks indicated by green circles and S2-wave velocity picks indicated by blue triangles (top right). Error bars for each pick indicated by a line in top two figures. The straight lines connecting the observed velocity values at each orientation is the best fitting curve, not predictions. Example P-wave seismogram depicts three different locations for velocity picks (bottom). The range of error varies based on the two other velocity picks shown in red on the seismogram. The relatively circular shape shown above and the fact that velocities do not vary by more than 250 m/s between orientations, indicates that this sample is classified as isotropic.

4. COMPARING STATIC AND DYNAMIC YOUNG'S MODULUS AND POISSON'S RATIO

Here we present evidence from calculations and laboratory experiments that compare dynamic and static Young's Modulus and Poisson's ratio values. Using radial velocity measurements and the Unistress cycle from static mechanical testing, dynamic and static values of E and n are determined, respectively.

Using radial P-wave and average S-wave velocity measurements, dynamic E and n can be calculated using Equations 1 and 2, respectively, for isotropic samples (Kuttruff, 1991). An average value of P-wave and S-wave velocity from the four radial velocity measurements were used to obtain a single value of E and n for each plug specimen. Each sample was plotted to compare resulting values and compare amongst rock types (Figures 12 and 13). TrJn samples had a dynamic Young's Modulus (E_d) that ranged from about 78 GPa to 86 GPa and a dynamic Poisson's ratio (n_d) that ranged from 0.19 to 0.23. Tpb' samples had an E_d that ranged from about 28 GPa to 42 GPa and a n_d that ranged from 0.26 to 0.28. Tss has an E_d that ranged from 57 GPa to 58 GPa and a n_d that ranged from 0.24 to 0.25. Therefore, we see here that the lithologic unit, TrJn, has the highest Young's Modulus and the lithologic unit, Tpb', has the highest value of Poisson's ratio. Tpb' samples contain numerous voids of ranging sizes (Table 4).

$$E_d = \rho V_s^2 \left[\frac{3V_p^2 - 4V_s^2}{V_p^2 - V_s^2}\right] \quad (1)$$

where E_d, ρ, V_p, V_s are dynamic Young's Modulus, sample density, P-wave velocity, and average S-wave velocity, respectively.

$$n_d = \frac{V_p^2 - 2V_s^2}{2(V_p^2 - V_s^2)} \quad (2)$$

where n_d, V_p, V_s are dynamic Poisson's ratio, P-wave velocity, and average S-wave velocity, respectively.

Using the Unistress cycle from static mechanical testing, static E and n is measured. Each sample was plotted to compare resulting values and compare amongst rock types (Figures 12 and 13). TrJn samples had a static Young's Modulus (E_s) that ranged from 52 GPa to 90 GPa and a static Poisson's ratio (n_s) that ranged from 0.14 to 0.17 based on measurements from three different plug sample of 21KF03. Tpb' samples had an E_s of about 35 GPa and a n_s of about 0.21 based on measurements from one plug sample of 21KF06. Lastly, Tss samples had an E_s of about 71 GPa and a n_s of about 0.09 based on measurements from one plug sample of 21KF20. Therefore, we see here that the lithologic units, TrJn and Tss, have the larger values of Young's Modulus and the lithologic unit, Tpb', has the highest value of Poisson's ratio (Table 4).

Relatively large differences between static and dynamic elastic properties are observed but consistent with literature. Between static and dynamic E and n values of TrJn the largest difference of E is about 34 GPa and the largest difference of n is about 0.09. For Tpb' samples, the largest difference between static and dynamic values was about 7 GPa for E and about 0.07 for n. For Tss samples, the largest difference between static and dynamic values was about 14 GPa for E and about 0.16 for n.

Table 4. Summary table for dynamic and static Young's Modulus (E) and Poisson's ratio (n) values from three different velocity pick locations. Dynamic E and n values calculated using 1 and 2, respectively. Static E and n values measured using Unistress cycle from static mechanical testing. E values are in GPa and n values are unitless. See Figure 11 (bottom seismogram image) for example of three ultrasonic velocity pick locations.

Specimen ID	Pick	Dynamic E [GPa]	Dymanic n	Static E [GPa]	Static n
03-03	1	84	0.22	57	0.14
	2	85	0.23		
	3	83	0.22		
03-04	1	78	0.23	90	0.17
	2	79	0.23		
	3	77	0.22		
03-05	1	86	0.19	52	0.16
	2	95	0.08		
	3	90	0.08		
06-01	1	42	0.28	35	0.21
	2	39	0.28		
	3	41	0.28		
06-02	1	28	0.26	N/A	N/A
	2	28	0.27		
	3	26	0.24		
20-01	1	58	0.24	N/A	N/A
	2	59	0.24		
	3	56	0.21		
20-02	1	58	0.24	71	0.09
	2	60	0.24		
	3	57	0.22		
20-03	1	57	0.25	N/A	N/A
	2	59	0.25		
	3	56	0.23		

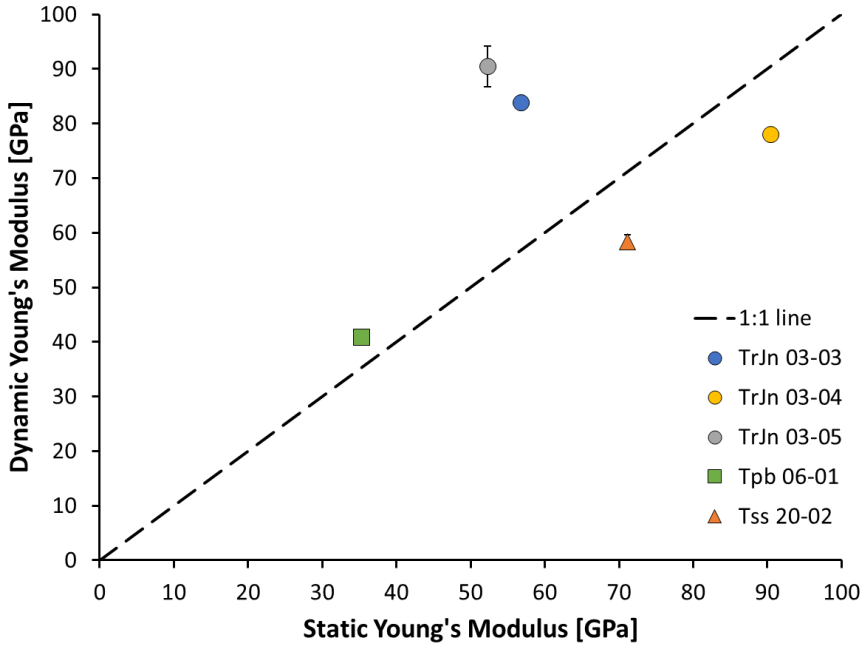

Figure 12. Average dynamic and static Young's Modulus used for each plug specimen. Plug specimens are categorized by lithologic unit: circles indicating TrJn specimens, squares indicating Tpb' specimens, and triangles indicating Tss specimens. The dashed black line represents a static to dynamic ratio of 1. Samples that are over this 1:1 line have a dynamic E that is greater than the static E, and vice versa.

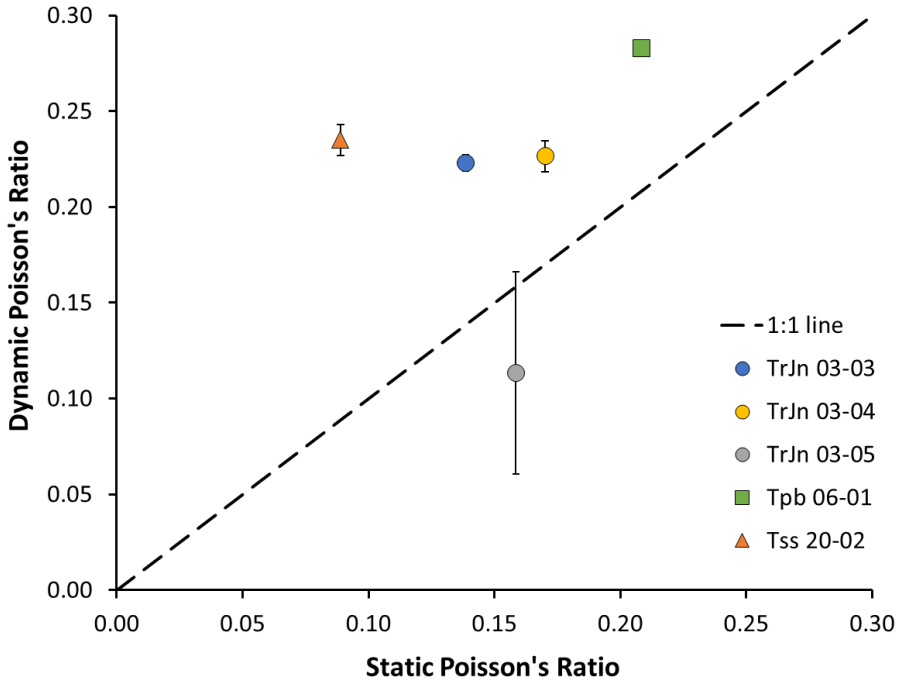

Figure 13. Average dynamic and static Poisson's Ratio used for each plug specimen. Plug specimens are categorized by lithologic unit: circles indicating TrJn specimens, squares indicating Tpb' specimens, and triangles indicating Tss specimens. The dashed black line represents a static to dynamic ratio of 1. Samples that are over this 1:1 line have a dynamic n that is greater than the static n, and vice versa.

5. CONCLUSIONS

In this study, we presented laboratory evidence that was used to classify samples taken from surface outcrops at San Emidio, Nevada, United States. Samples were classified as either isotropic or anisotropic and/or contained heterogeneities based on radial velocity measurements and geological/textural observations made from thin sections. By classifying these plug specimens before future data analysis, we can properly obtain the correct number of independent elastic constants needed to fully characterize each plug specimen. We also show the observed differences between static and dynamic moduli, which is important when the stress model incorporates dynamic well log estimations of elastic modulus. Many challenges were encountered through the process of identifying anisotropy and/or heterogeneities within a specimen. If needed, additional samples will be prepared to further investigate anisotropy and to better calculate independent elastic constants. The next steps after mechanical and poroelastic testing is to achieve associated stiffnesses and Biot coefficients for each lithologic unit. In addition, measurements will be made at multiple stresses to also determine if stress-induced anisotropy exists, even for initially isotropic materials.

ACKNOWLEDGEMENTS

We would like to thank the following individuals for their assistance in collecting samples from the field: Matthew Folsom, Chris Gates, Quaid Ricks, and Neal Lord. We are also extremely grateful for the Ormat staff members for their assistance in this project.

This work has been recommended by the Geothermal Technologies Office of the U.S. Department of Energy. The WHOLESCALE work in this study is supported by the U.S. Department of Energy, Office of Energy Efficiency and Renewable Energy (EERE), under Award Numbers DE-EE0007698 and DE-EE0009032. We wish to recognize the WHOLESCALE Team members for providing motivation and feedback.

WHOLESCALE Team: K.L. Feigl, J. Akerley, S. Batzli, S. Bradshaw, M.A. Cardiff, E. Cunningham, M. Cusini, M. Di Donato, M. Folsom, H. Guo, J. Hampton, B. Heath, B. Jahnke, S.J. Kleich, C. Kreemer, N.E. Lord, B. Pecoraro, Q. Ricks, C. Roland, C. Sherman, H. Sone, C.H. Thurber, S. Tung, H.F. Wang, I. Warren

REFERENCES

Drakos, P. S. (2007). Tertiary stratigraphy and structure of the southern Lake Range northwest Nevada: Assessment of kinematic links between strike-slip and normal faults in the northern Walker Lane (Doctoral dissertation, University of Nevada, Reno).

Faulds, J. E., Henry, C. D., & Hinz, N. H. (2005). Kinematics of the northern Walker Lane: An incipient transform fault along the Pacific–North American plate boundary. Geology, 33(6), 505-508.

Faulds, J. E., Coolbaugh, M. F., Vice, G. S., & Edwards, M. L. (2006). Characterizing structural controls of geothermal fields in the northwestern Great Basin: A progress report. Geothermal Resources Council Transactions, 30, 69-76.

Feigl, K. L. & WHOLESCALE Team. (2020). Spatio—Temporal Analysis of Deformation at San Emidio Geothermal Field, Nevada, USA between 1992 and 2010, Proceedings, 45th Workshop on Geothermal Reservoir Engineering, Stanford University, Stanford, California.

Feigl, K. L. & WHOLESCALE Team. (2022). Overview and Preliminary Results from the WHOLESCALE project at San Emidio, Nevada, U.S., Proceedings, 47th Workshop on Geothermal Reservoir Engineering, Stanford University, Stanford, California.

Folsom, M., Libbey, R., Feucht, D., Warren, I., Garanzini, S. (2020). Geophysical Observations and Integrated Conceptual Models of the San Emidio Geothermal Field, Nevada, Proceedings, 45th Workshop on Geothermal Reservoir Engineering, Stanford University, Stanford, California.

Kuttruff, H. (1991). Ultrasonics: Fundamentals and Applications. Elsevier Science Publishers, Essex, England.

Matlick, S. (1995). San Emidio Geothermal System, Empire, NV. GRC Field Trip – October 1995. Mesquite Group, Inc.

Rhodes, G.T., Faulds, J. E. & Teplow, W. (2010). Structural Controls of the San Emidio Geothermal Field, Northwestern Nevada, 390 Geothermal Resource Council Transactions, Vol. 34.

Rhodes, G. T., Faulds, J. E., & Ramelli, A. R. (2011) Preliminary Geologic Map of the Northern Lake Range, San Emidio Geothermal Area, Washoe County, Nevada. Nevada Bureau of Mines and Geology, Open-File report, 11-11.

Teplow, W. J., & Warren, I. (2015). Finding Large Aperture Fractures in Geothermal Resource Areas Using a Three-Component Long-Offset Surface Seismic Survey, PSInSAR and Kinematic Structural Analysis (No. DOE-US Geothermal Inc-0002847). US Geothermal, Inc., Boise, Idaho, United States.